Supplementary Information

ParSE-seq: a calibrated multiplexed assay to facilitate the clinical classification of putative splice-altering variants

Supplementary Inventory/Table of Contents

Supplementary Table 6. Electrophysiology Data for two Na$_v$1.5 variants.
Supplementary Table 7. Passive parameters of CRISPR-edited iPSC-CMs.

Supplementary Data 1. Reagents, manufacturer, and catalogue numbers.
Supplementary Data 2. Variant characteristics – genomic position, gnomAD allele frequency, ClinVar classification, and SpliceAI prediction.
Supplementary Data 3. ParSE-seq functional iPSC-CM and HEK data for all studied variants.

Supplementary References.

Supplementary Methods

Description of Next Generation Sequencing datasets used in this study. The following are descriptions of the NGS datasets used in the ParSE-seq manuscript. All DNA sequencing data are available at https://www.ncbi.nlm.nih.gov/bioproject/?term=PRJNA1106089.

MO-9293 – PacBio long-read sequencing dataset for assembly.

MO-9402 – Illumina short-read sequencing of barcode frequency from barcoded plasmid pool. Used to compare barcode abundance based on long-read sequencing and short read sequencing (Supplementary Figure 2).

MO-9419 – Illumina short-read sequencing of assay performed in triplicate in iPSC-CMs.

MO-9489 – Illumina short-read sequencing of assay performed in triplicate in HEK cells.

MO-9518 – Illumina RNA-seq data for wildtype iPSC-CMs treated with CHX and DMSO.

MO-9872 – Illumina RNA-seq data for heterozygous c.1891-5G>C iPSC-CMs treated with CHX and DMSO.

MO-10995 – Illumina RNA-seq data for heterozygous c.4220G>C iPSC-CMs treated with CHX and DMSO.

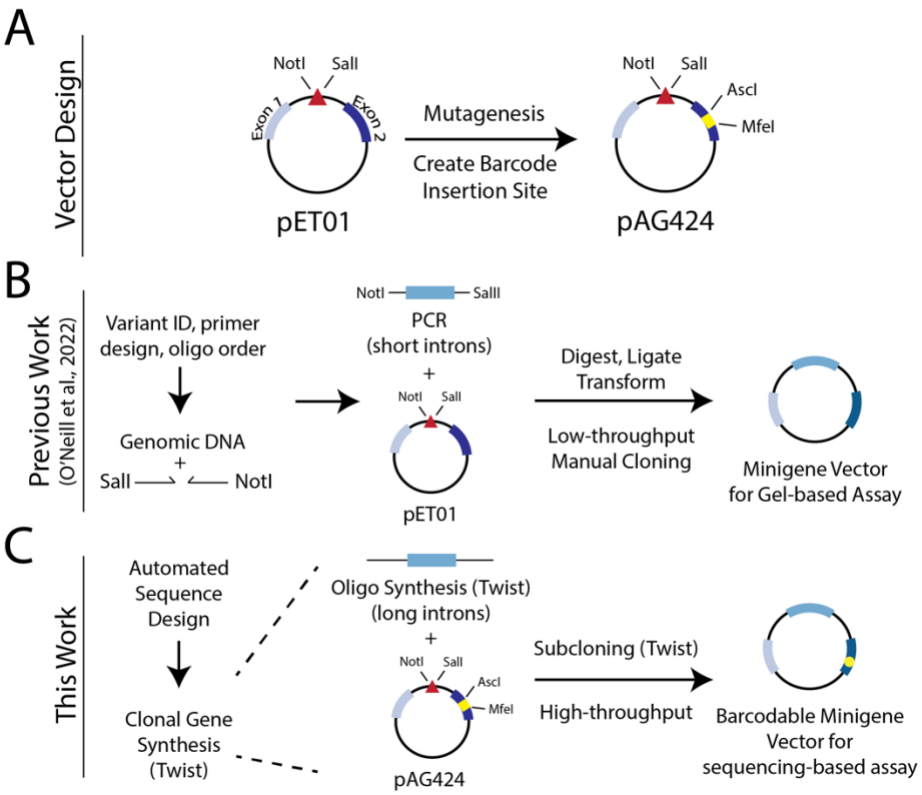

Supplementary Figure 1. Schematic of vector design and cloning overview.
A) pET01 is an established minigene vector containing a MCS between rat insulin exon 1 and 2 and flanking intronic sequences (MoBiTec GmbH). PCR-mutagenesis was used to create a new restriction site in rat insulin exon 2 to allow downstream insertion of a barcode.
B) Schematic of our previous workflow for manual minigene assays using gel-based quantification and manual cloning[1].
C) Schematic of current approach for high-throughput sequencing-based quantification of splicing. pAG424 was sent to Twist Biosciences, and non-restriction-based cloning of chemically synthesized oligonucleotides was performed.

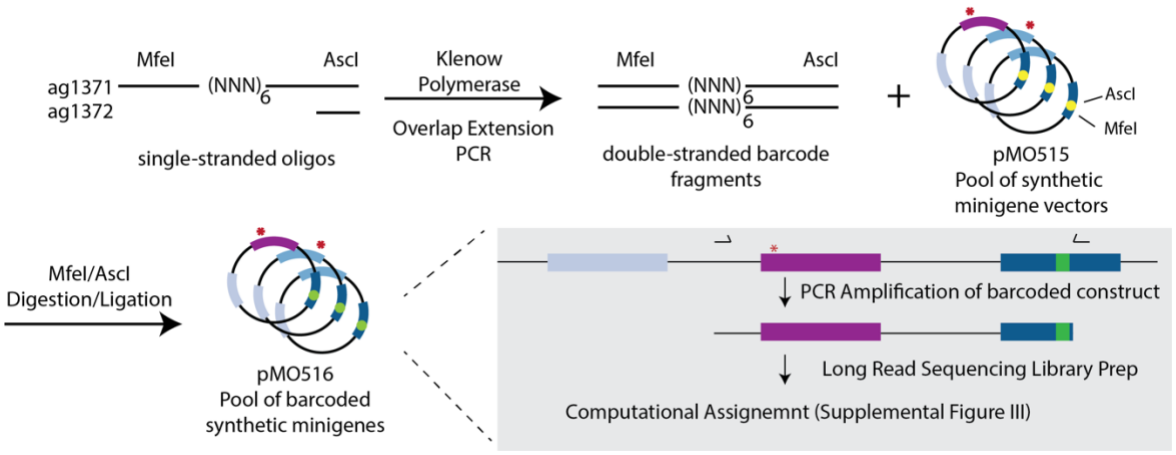

Supplementary Figure 2. Barcode cloning schematic. Molecular barcodes (represented by NNN) were created from two single-stranded oligonucleotides, which were annealed and underwent PCR overlap extension. Following purification, oligonucleotides were digested and ligated to a digested pool of minigene vectors (pMO515; yellow dot barcode digestion site pre-insertion). Multiple dilutions of barcodes were tested to arrive at a barcoded pool (pMO516; green dot barcode digestion site post-insertion), with each unique vector covered by a median of 11 barcodes. Experimentally, barcode assignment was completed with PCR amplicons from this pool. Long-read sequencing libraries were prepared from these amplicons, after which computational analyses presented in the methods, GitHub, and Supplementary Figure 3 enabled unique assignments.

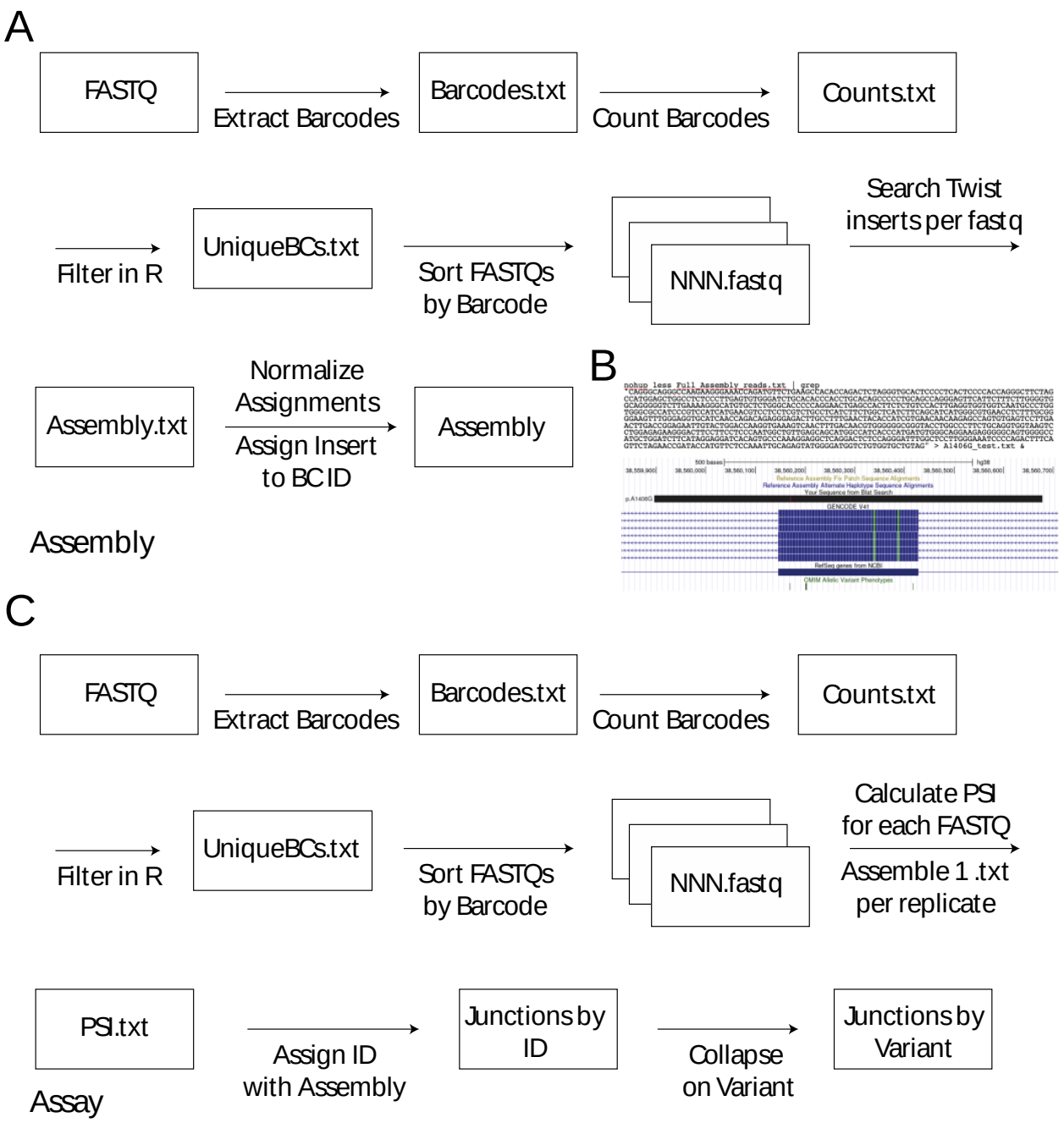

Supplementary Figure 3. Schematic of assay and assembly computational workflows.
A) Assembly process from raw FASTQ to assembly cipher.
B) Genome Browser representation of searched Twist insert showing variant.
C) Assay process from raw FASTQ to processed reads per variant. PSI indicates Percent Spliced In.

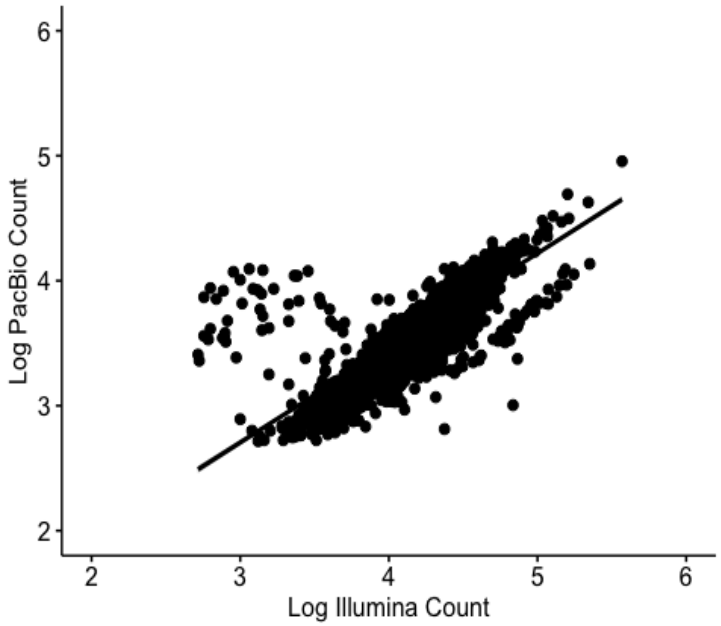

Supplementary Figure 4. Library barcode frequency by Illumina and PacBio sequencing methods. Pearson correlation of barcode counts of pooled barcoded plasmids by Illumina sequencing and PacBio sequencing. Each dot represents one unique barcode captured in both Illumina and PacBio libraries (N = 3290). P-values were calculated by a Pearson correlation test (2-sided), exact p = 4.04 e-125. Raw data in Source Code.

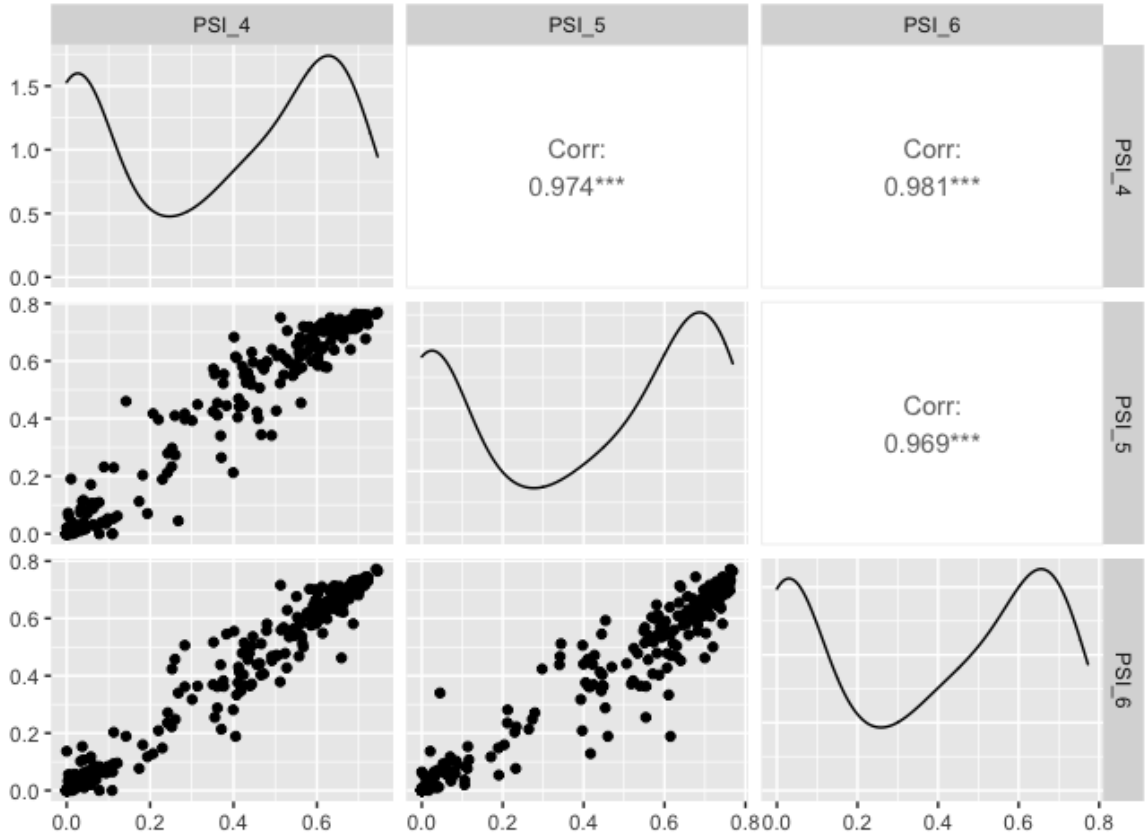

Supplementary Figure 5. PSI correlations among HEK replicates. Spearman correlations among ParSE-seq replicates in HEK cell assay experiments using ggpairs function in R (N=244). Raw data in Supplementary Data 3. X- and Y-axes correspond to ΔPSI_norm from each replicate.

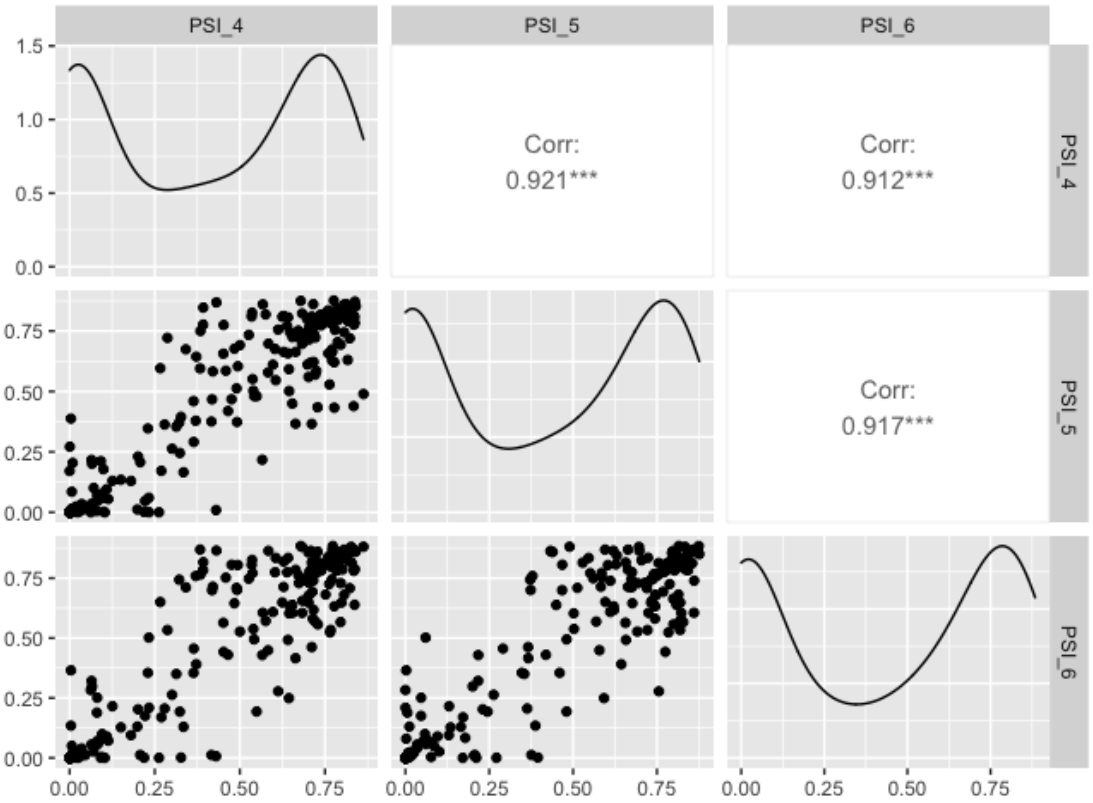

Supplementary Figure 6. PSI correlations among iPSC-CM replicates. Spearman correlations among ParSE-seq replicates in iPSC-CMs assay experiments using ggpairs function in R (N = 224). Raw data in Supplementary Data 3. X- and Y-axes correspond to ΔPSI_norm from each replicate.

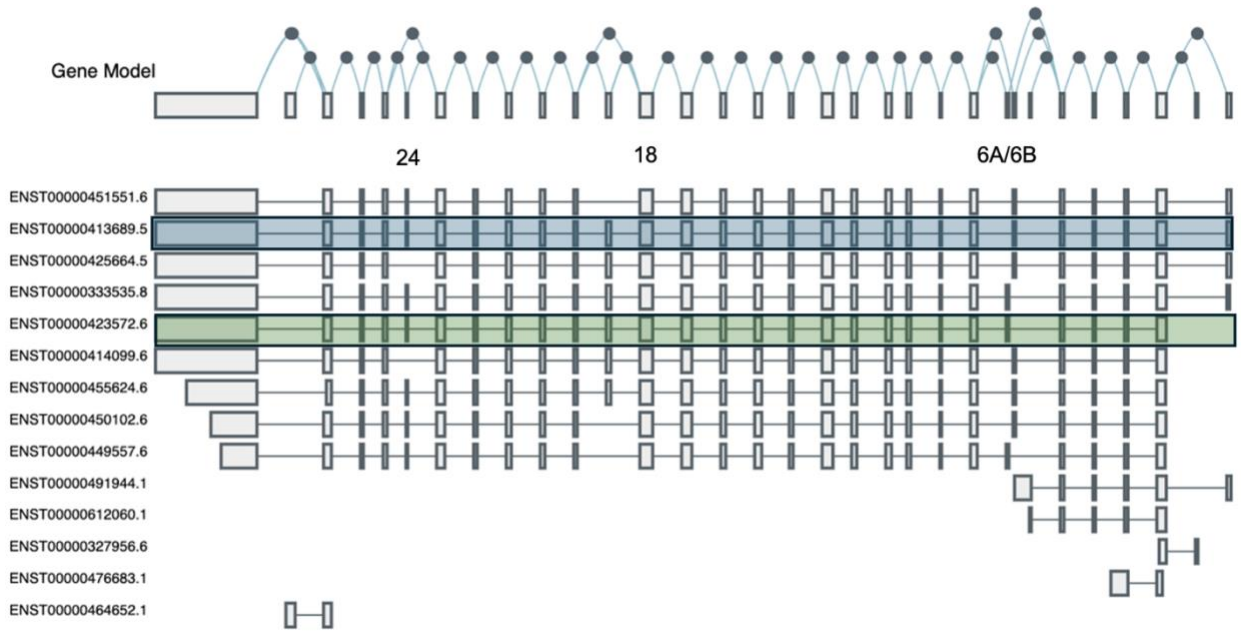

Supplementary Figure 7. *SCN5A* transcript alternative splicing patterns from the Genotype Tissue Expression Database (GTEx). *SCN5A* is transcribed right to left, across exons 1-28. Clinically relevant transcripts are ENST00000423572.6 (Green; MANE select) and ENST00000413689.6 (Blue; MANE clinical plus). The alternative spliced exons 6A/6B, 18, and 24 are depicted above the transcript tracks. Data was directly obtained at the GTEx online portal[2].

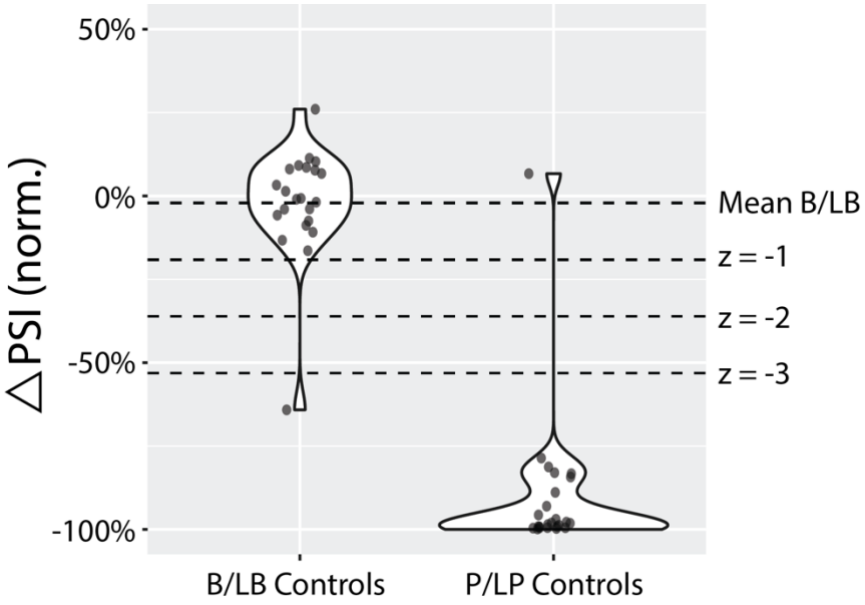

Supplementary Figure 8. Calibration of Thresholds for Functional Outcomes. We calculated the ΔPSI_norm in iPSC-CMs of B/LB control variants and derived the mean score and standard deviation for annotating additional variants. We observe excellent stratification of B/LB (N = 22; Benign/Likely Benign controls) and P/LP variants (N = 25; Pathogenic/Likely Pathogenic controls). Raw data in Supplementary Data 3.

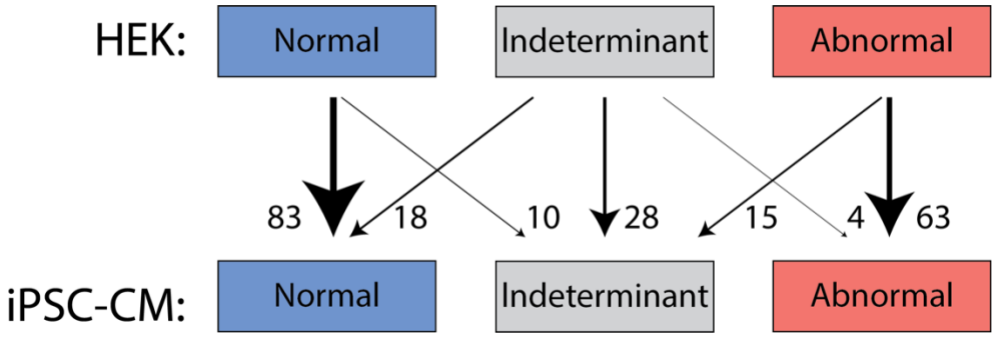

Supplementary Figure 9. Variant interpretations between HEK and iPSC-CM assays. There were no variants with a normal score in one cell type and an abnormal score in the other cell type. Variant outcomes present in Supplementary Data 3. HEK – Human Embryonic Kidney cell; iPSC-CM – induced pluripotent stem cell-cardiomyocyte.

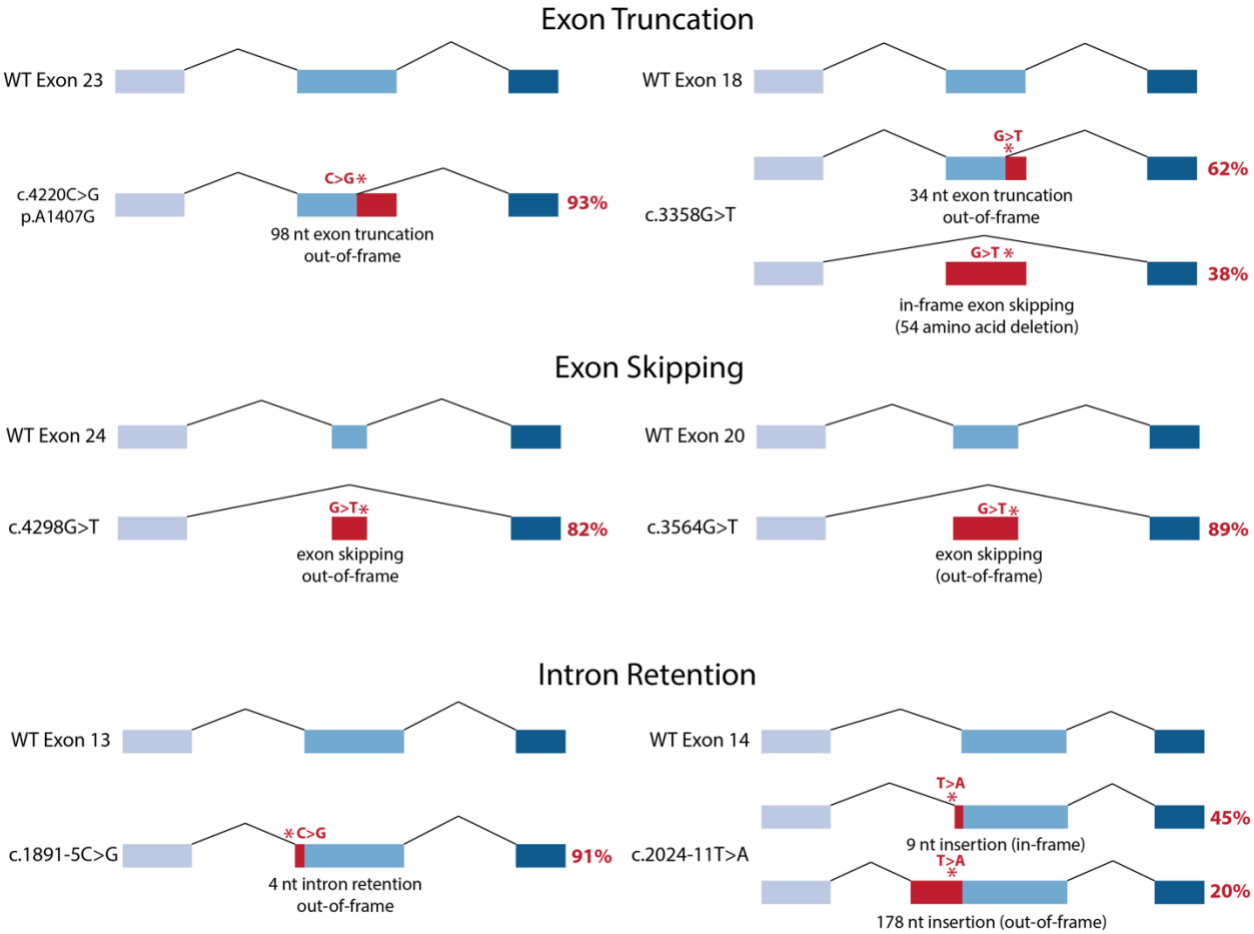

Supplementary Figure 10. Molecular impact of splice-altering variants. ParSE-seq captures exon truncation, exon skipping, and intron retention events. Multiple aberrant splicing events were occasionally observed for a single variant. Splicing outcomes in Supplementary Data 3.

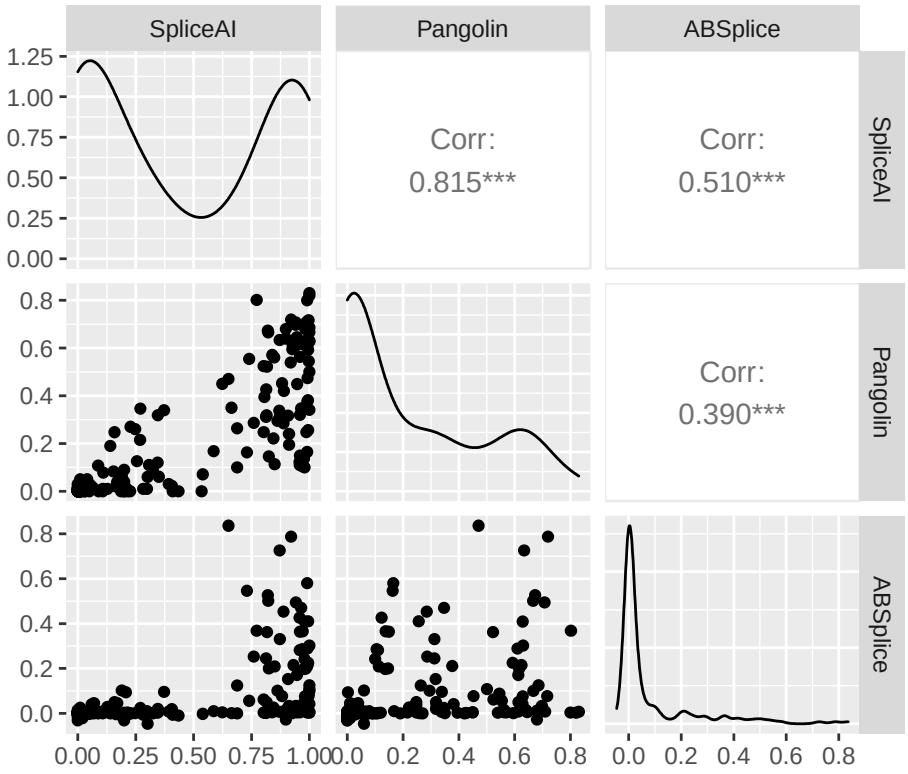

Supplementary Figure 11. Spearman correlations of predictions for SpliceAI, Pangolin, and AbSplice for all variants. To better understand variant effect predictor performance on functional outcomes, we first tested correlation among three variant prediction tools for the ParSE-seq library. Each dot represents an individual variant with relative scores from each variant effect predictor. X- and Y-axes correspond to ΔPSI_norm from each replicate. Correlations were performed using a Spearman analysis in R. Raw scores are present in Supplementary Data 2.

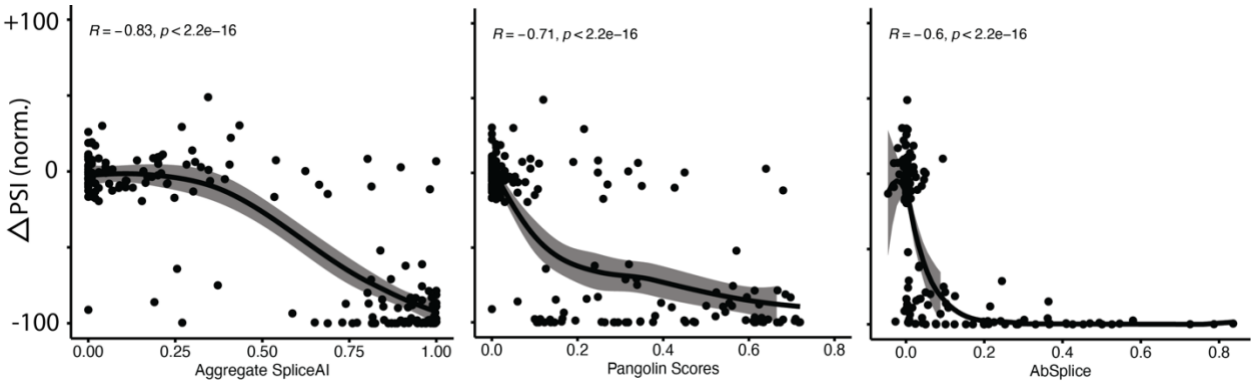

Supplementary Figure 12. Variant effect predictor correlation with ParSE-seq outcomes. Spearman rho correlations for SpliceAI scores (N=181; p=3.87e-47), Pangolin scores (N=182; 3.56e-30), and ABSplice scores (N=178; 1.23-e18) with ΔPSI_norm across all experimental variants, including canonical splice sites. P-values were determined using a Pearson correlation. Raw data available in Source Code and Supplementary Data 3.

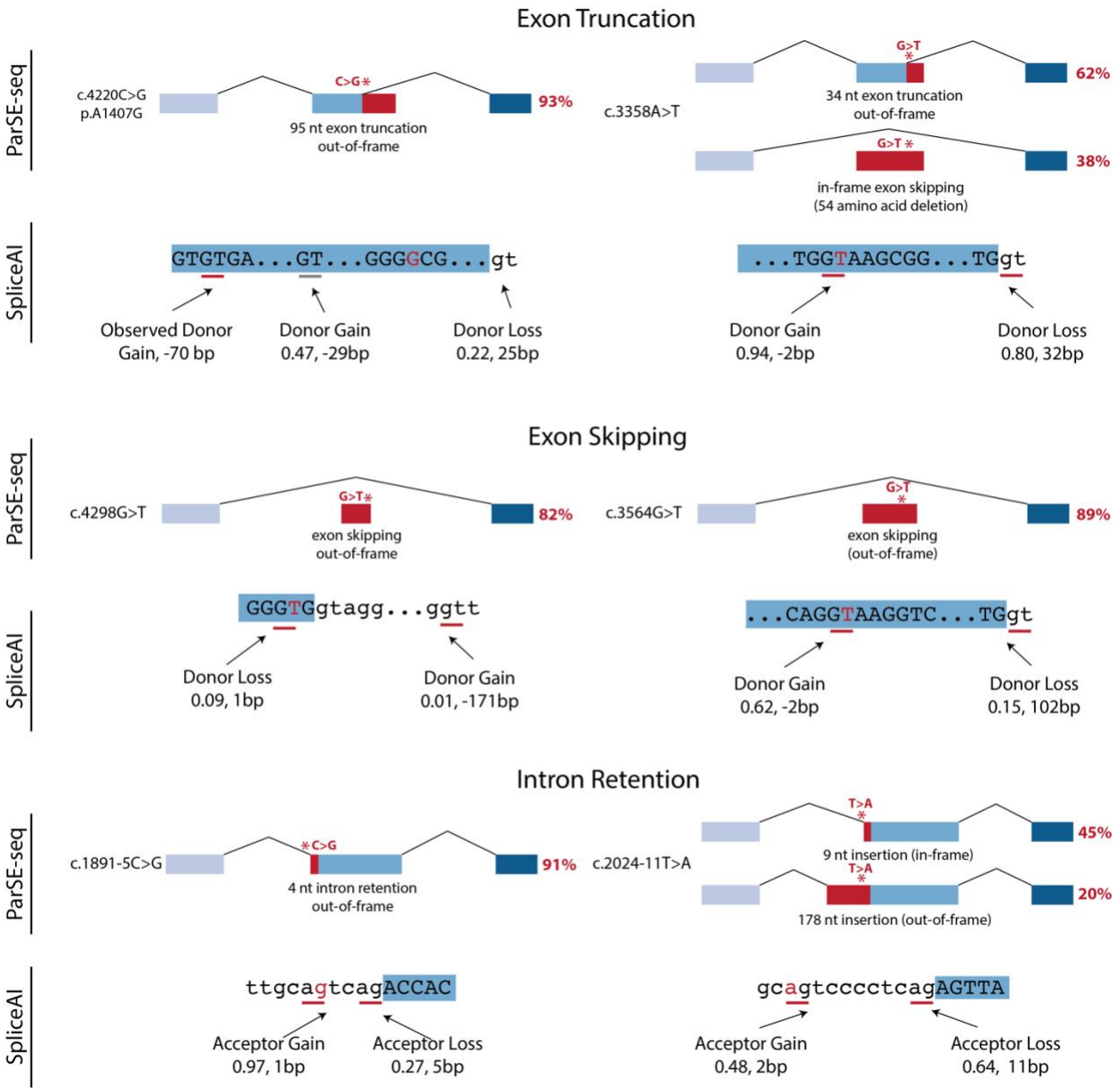

Supplementary Figure 13. SpliceAI predictions and ParSE-seq molecular outcomes. We compared ParSE-seq experimental outcomes (top) with SpliceAI predictions for donor/acceptor loss/gain (bottom) across three different molecular events. SpliceAI gives one prediction for each variant, where some variants led to both the SpliceAI prediction and exon skipping. SpliceAI predictions typically matched experimental data for activation of cryptic splice sites (c.3358A>T, c.1891-5C>G, c.2024-11T>A), although in the ParSE-seq assay a different cryptic site may be activated (c.4220C>G) or exon skipping may predominate (c.4298G>T and c.3564G>T). Splicing outcomes in Supplementary Data 3.

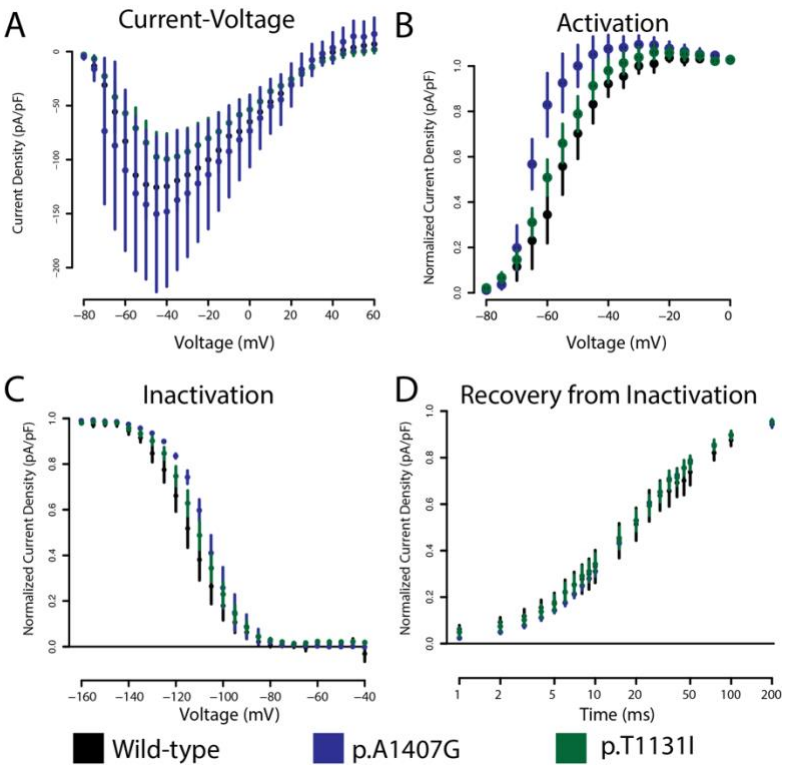

Supplementary Figure 14. Electrophysiological parameters of suspected splice-altering missense variants in a cDNA high-throughput automated patch-clamp assay. Raw EP data is available in Source Code for each protocol. Black indicates WT, blue p.A1407G, and green p.T1131I.

A) Current-Voltage (IV) curve for two splice-altering missense variants. Distributions of currents overlap between WT (black; N = 90), p.A1407G (blue; N = 46), and p.T1131 (green, n = 67) across the tested range of voltages.

B) Activation curve for the WT $Na_V1.5$ and two missense variants. WT (black; N = 7), p.A1407G (blue; N = 6), and p.T1131 (green, n = 16). A small left-shift of activation is observed for p.A1407G (phenotypic gain-of-function).

C) Inactivation curve for WT $Na_V1.5$ and two missense variants. WT (black; N = 11), p.A1407G (blue; N = 5), and p.T1131 (green, n = 20). A right-shift of inactivation is observed for p.A1407G (phenotypic gain-of-function).

D) Recovery from inactivation for WT $Na_V1.5$ and two missense variants. WT (black; N = 11), p.A1407G (blue; N = 5), and p.T1131 (green, n = 18).

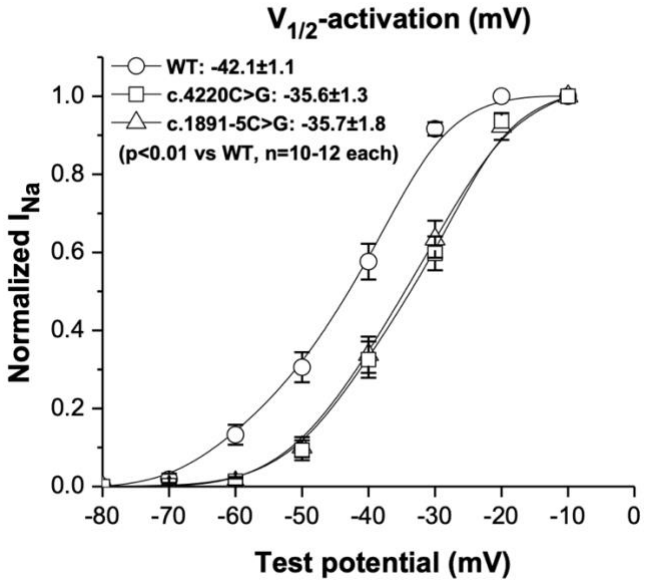

Supplementary Figure 15. Voltages of half-activation for iPSC-CM models. Error bars indicate standard error of the mean. Values were compared with a two-tailed t-test. Comparisons across biological replicates of WT (N = 10), c.4220C>G (N = 10), and c.1891-5C>G (N=12). Raw data available in Supplementary Table 7.

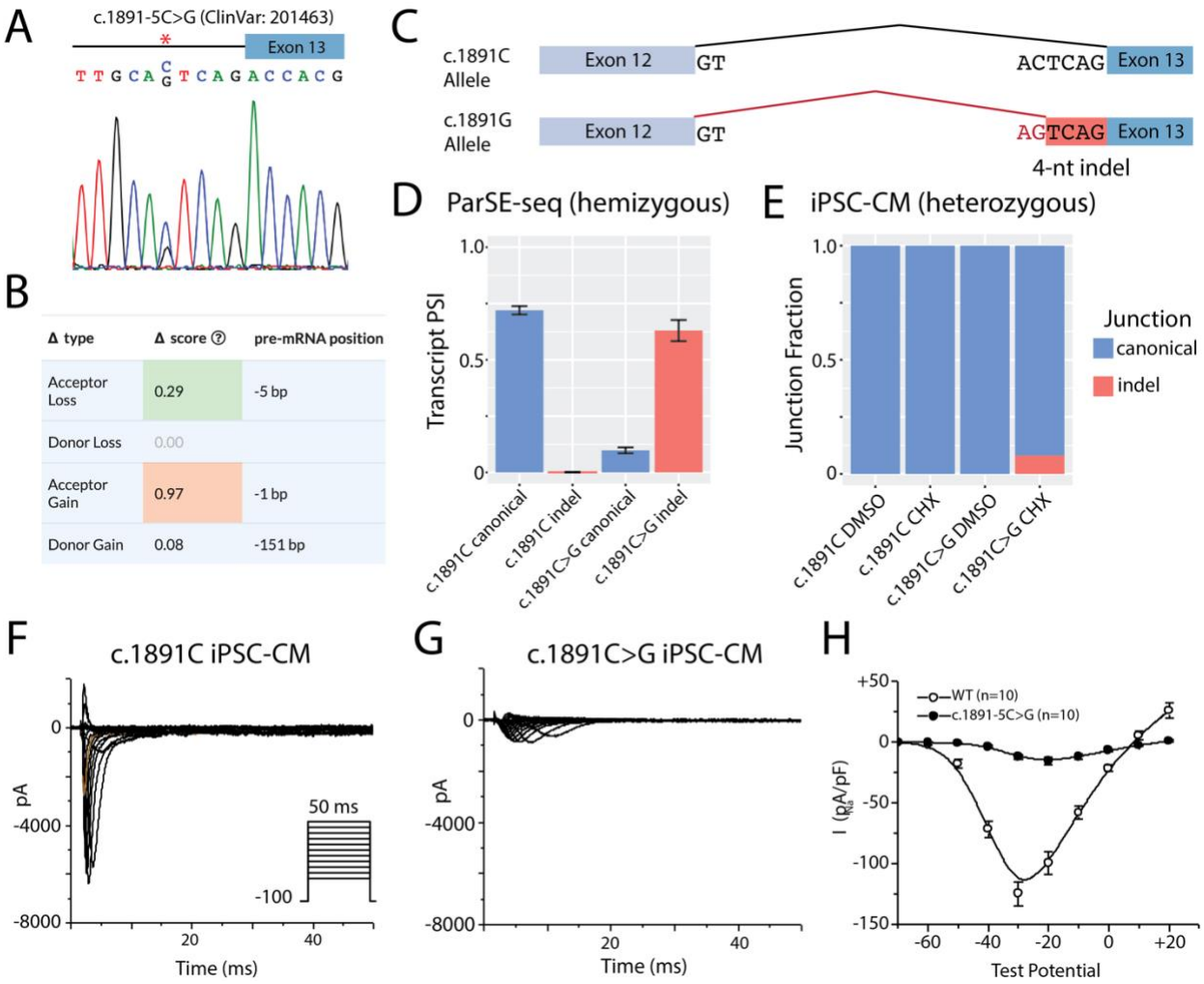

Supplementary Figure 16. Intronic variant at the endogenous *SCN5A* locus disrupts *SCN5A* RNA splicing and protein-level sodium current.

A) The c.1891-5C>G variant was introduced as a heterozygous edit with CRISPR-Cas9 into a control iPSC line. Both control and edited lines underwent differentiation to iPSC-CMs.

B) Variant level SpliceAI predictions of the c.1891C>G variant. New motif is predicted to abolish canonical splice site and introduce a novel splice site at the *de novo* AG motif. Screenshot obtained from https://spliceailookup.broadinstitute.org/.

C) Schematic depiction of splicing outcomes for the WT allele and variant allele. The variant allele is predicted to use a cryptic splice site and retain 4 nucleotides of intronic sequence as a frame-shifting indel.

D) Hemizygous ParSE-seq results of the PSI for the WT splicing product vs the specifically predicted 4-bp indel created by the competing AG motif in the WT and variant constructs. Transcript PSI quantified for >50 across 11 barcodes for c.1891 and 28 barcodes for WT. Blue indicates canonical splicing and red aberrant splicing of 4-nt insertion. Error bars correspond to standard error of the mean. Raw data in Source Code.

E) Fraction of canonical vs ParSE-seq predicted indel in WT lines and heterozygous edited lines. Blue indicates canonical splicing and red aberrant splicing of 4-nt insertion. Reads correspond to hundreds of *SCN5A* reads (see Supplementary Methods). Raw counts from NIH BioProject accession #1106089.

F) Sodium current traces of the healthy control line, representative traces from a single cell recording. Voltage protocol provided in inset. Representative currents from a single cell in Supplementary Table 7.
G) Sodium current traces of the heterozygous c.1891C>G line, representative traces from a single cell recording. Same voltage protocol as in F. Representative currents from a single cell in Supplementary Table 7.
H) Quantification of peak current at -30 mV of the isogenic lines. $p < 0.01$ (2-sided t-test). Error bars indicate standard error of the mean. Averaged peak currents (from F and G) in 10 biological replicates of each cell type. Data in Supplementary Table 7.

Supplementary Table 1. Construct exon and flanking intron lengths. Constructs were manually designed using the ENST00000333535 *SCN5A* transcript. We aimed for 250 flanking intronic nucleotides on each end of the exon. For certain exons, we were limited with overlap from adjacent exons or from high GC content in the intronic regions, complicating oligo synthesis. In addition, *SCN5A* uses 2 instances of non-canonical AC/AT splice sites between exons 3 and 4, and exons 25 and 26, so we did not study those constructs. All complete sequences are present in Supplementary Data 2.

Construct	Exon BPs	Upstream BPs	Downstream BPs
5	129	250	250
6	92	100	152
7	231	250	250
8	64	250	250
9	142	250	250
10	198	125	125
11	180	250	250
12	372	125	125
13	133	250	250
14	239	250	250
16	351	250	250
18	162	250	250
19	121	250	250
20	155	250	250
21	174	250	250
22	123	250	250
23	282	250	250
24	54	250	250
27	271	250	250

Supplementary Table 2. Primers used in this study. All primers were ordered from Sigma, or Integrated DNA Technologies (all primers >50 nts long).

Primer	Sequence	Description
ag1799	CAAGCAGAAGACGGCATACGAGATCGGTCCGATAGTGACTGGAGTTCAGAC GTGTGCTCTTCCGATCTGCGTGGATTCTTCTACACACCC	Illumina I7 primer
ag1800	CAAGCAGAAGACGGCATACGAGATGCCGGCGTATGTGACTGGAGTTCAGAC GTGTGCTCTTCCGATCTGCGTGGATTCTTCTACACACCC	Illumina I7 primer
ag1801	CAAGCAGAAGACGGCATACGAGATATTAATACGCGTGACTGGAGTTCAGAC GTGTGCTCTTCCGATCTGCGTGGATTCTTCTACACACCC	Illumina I7 primer
ag1802	CAAGCAGAAGACGGCATACGAGATGTTGTGTAACGTGACTGGAGTTCAGAC GTGTGCTCTTCCGATCTGCGTGGATTCTTCTACACACCC	Illumina I7 primer
ag1803	CAAGCAGAAGACGGCATACGAGATACCACACGGTGTGACTGGAGTTCAGAC GTGTGCTCTTCCGATCTGCGTGGATTCTTCTACACACCC	Illumina I7 primer
ag1804	CAAGCAGAAGACGGCATACGAGATTTGTAGTGTAGTGACTGGAGTTCAGAC GTGTGCTCTTCCGATCTGCGTGGATTCTTCTACACACCC	Illumina I7 primer
ag1805	CAAGCAGAAGACGGCATACGAGATCCACGACACGGTGACTGGAGTTCAGAC GTGTGCTCTTCCGATCTGCGTGGATTCTTCTACACACCC	Illumina I7 primer
ag1806	CAAGCAGAAGACGGCATACGAGATGGCAGTAGCAGTGACTGGAGTTCAGAC GTGTGCTCTTCCGATCTGCGTGGATTCTTCTACACACCC	Illumina I7 primer
ag1807	CAAGCAGAAGACGGCATACGAGATAATGACGATGGTGACTGGAGTTCAGAC GTGTGCTCTTCCGATCTGCGTGGATTCTTCTACACACCC	Illumina I7 primer
ag1808	CAAGCAGAAGACGGCATACGAGATTTGACCAATGGTGACTGGAGTTCAGAC GTGTGCTCTTCCGATCTCTGGATTGTCCTATGTGTCTTGCTT	Illumina i7 primer
ag1809	AATGATACGGCGACCACCGAGATCTACACGAGCGACGATACACTCTTTCCCT ACACGACGCTCTTCCGATCTGGGCCACCTCCAGTGC	Illumina i5 primer
ag1646	AATGATACGGCGACCACCGAGATCTACACCCGTATGTTCACACTCTTTCCCT ACACGACGCTCTTCCGATCTGGGCCACCTCCAGTGC	Illumina I5 Primer
ag1647	AATGATACGGCGACCACCGAGATCTACACAAGATACACGACACTCTTTCCCT ACACGACGCTCTTCCGATCTGGGCCACCTCCAGTGC	Illumina I5 Primer
ag1648	AATGATACGGCGACCACCGAGATCTACACGGAGCGTGTAACACTCTTTCCCT ACACGACGCTCTTCCGATCTGGGCCACCTCCAGTGC	Illumina I5 Primer
ag1649	AATGATACGGCGACCACCGAGATCTACACATTGATACTGACACTCTTTCCCT ACACGACGCTCTTCCGATCTGGGCCACCTCCAGTGC	Illumina I5 Primer
ag1650	AATGATACGGCGACCACCGAGATCTACACGCCAGCGTCAACACTCTTTCCCT ACACGACGCTCTTCCGATCTGGGCCACCTCCAGTGC	Illumina I5 Primer
ag1651	AATGATACGGCGACCACCGAGATCTACACCACCGATGTGACACTCTTTCCCT ACACGACGCTCTTCCGATCTGGGCCACCTCCAGTGC	Illumina I5 Primer
ag1652	AATGATACGGCGACCACCGAGATCTACACTGTTAGCACAACACTCTTTCCCT ACACGACGCTCTTCCGATCTGGGCCACCTCCAGTGC	Illumina I5 Primer
ag1653	AATGATACGGCGACCACCGAGATCTACACTTGGCAGCGTACACTCTTTCCCT ACACGACGCTCTTCCGATCTGGGCCACCTCCAGTGC	Illumina I5 Primer
ag1654	AATGATACGGCGACCACCGAGATCTACACCCAATGATACACACTCTTTCCCT ACACGACGCTCTTCCGATCTGGGCCACCTCCAGTGC	Illumina I5 Primer
ag1371	ATTAGGCGCGCCGCGGCCGCNNNNNNNNNNNNNNNNNNNGTCGACCAATTG ATTA	pAG424 Barcode F
ag1372	TAATCAATTGGTCGAC	pAG424 Barcode R
ag491	TTCAGCAATTGGCACTGGAGGTGGCCC	Jain F pET01 barcode RE site
ag492	GGTGGCGCGCCTCCACCCAGCTCCAGTTGT	Jain R pET01 barcode RE site
mo38	GATCCACGATGC	pAG424 gene specific RT primer
mo37	GGATTCTTCTACACACCC	pAG424 seq primer F
ag489	GGGCCACCTCCAGTGC	pAG424 seq primer R
ag490	CTGGATTGTCCTATGTGTCTTTGCTTCT	pAG424 barcode seq primer F
mo367	CCCAGGGTGCGGTGAGATCCCAGAGGA	SCN5A QC SP T1131I
ag1749	TTGACAACGTGGGGGGCGGGTACCTGGC	SCN5A QC SP A1407G
mo346	CACCGTTGCACTCAGACCACGCCAT	c.1891-5C>G Guide F
mo347	AAACATGGCGTGGTCTGAGTGCAAC	c.1891-5C>G Guide R
mo348	TCGAAGCCATCTACACACGGAGCCTGGGAGGTCAGCATCTGGGGCCCGCCT GGCTCCTCTGATGGCGTGGTCTGACTGCAATCAGGAGATTTGCGTCAGCCT GGGGAAAAGGGTCCTGCCCCCAGCTCCTGTCCTGCTGGACCTGGGGAGG	c.1891-5C>G repair template with PAM break
mo198	GGAGGACCTGTGATATGTGTAGC	c.1891-5G>A genotyping F
mo199	AGATAGACATGGTTATGGTTGGGA	c.1891-5G>A genotyping R
mo359	CACCGCAACGTGGGGGCCGGGTACC	c.4220C>G Guide F
mo360	AAACGGTACCCGGCCCCCACGTTGC	c.4220C>G Guide R
mo361	CTGCTCAACAGCCATTGGGAGGAAGGAAGTCCCTTCTCTCCAGGACTTACCA CCTGCAGAAGGGCTAGGTACCCGCCCCCCACGTTGTCAAAGTTGACTTTCA CCTTGGTCCAGTACAATTCTCCGGTCAAGTTCAAGGACTCACACTGGC	c.4220C>G repair template with PAM break
mo362	GCCTCATCTTCTGGCTCATCT	c.4220C>G genotyping F
mo363	GATCCTCCTATGAAGATCCAGCA	c.4220C>G genotyping R

QC – QuikChange; SP – SyncroPatch. F – Forward. R — Reverse.

Supplementary Table 3 Sensitivity analysis of functionally abnormal/normal thresholds for control variants and total variant assignments in the iPSC-CM dataset. See Methods for derivations of OddsPath priors and posteriors. Indeterminant variants are those with normalized PSI changes that fall between the pathogenic or benign cutoffs. The primary analysis used in the paper is highlighted in bold. Raw data for calibration are from Supplementary Data 3.

Pathogenic Cutoff	Benign Cutoff	P1	P2path	P2benign	OddsPath_P	OddsPath_B	P Strength	B Strength	Assignable Variants
< -36	> -17	0.532	0.960	0.045	21.12	0.0419	PS3	BS3	179
< -72	> -17	0.543	0.96	0.045	20.16	0.04	PS3	BS3	172
< -36	> -36	0.5	0.96	0.040	24	0.0417	PS3	BS3	201
< -50	**> -20**	**0.532**	**0.960**	**0.045**	**21.12**	**0.0419**	**PS3**	**BS3**	**182**
< -40	> -20	0.532	0.960	0.045	21.12	0.0419	PS3	BS3	183
< -30	> -20	0.532	0.960	0.045	21.12	0.0419	PS3	BS3	183
< -20	> -20	0.532	0.960	0.045	21.12	0.0419	PS3	BS3	184

Supplementary Table 4. OddsPath Path calculations for ParSE-seq datasets. To calibrate our evidence strength, we used the Odds of Pathogenicity framework for benign and pathogenic variant functional data elaborated by Brnich et al[3]. We performed independent calibrations for variants studied in each cell type (iPSC-CM, top row; and HEK, bottom row). A represents benign controls with concordant functional outcomes, B benign with abnormal outcome, C pathogenic controls with normal outcome, and D, pathogenic controls with concordant outcomes. P1 is a prior based on control counts, P2 is a posterior based on outcomes, and OP represents transformed OddsPath for each category (Benign and Pathogenic). Please see methods for full descriptions of the methodology.

Dataset	A	B	C	D	P1	P2_P	P2_B	OP_P	OP_B	ACMG_P	ACMG_B
CM_final	21	1	1	24	0.53	0.96	0.045	21.3	0.042	strong	strong
HEK_final	27	0	1	30	0.53	0.97	0.036	28.7	0.033	strong	strong

Supplementary Table 5. ACMG criteria for variant interpretation. We followed the 2015 ACMG guidelines for variant interpretation, with the functional evidence calibration 'OddsPath' described in the methods. CI indicates conflicting interpretation, AC allele count, and AF allele frequency. Evidence scores were derived from calibrated functional data (PS3/BS3), *in silico* predictors (PP3/BP4), and gnomAD allele count (PM2).

HGVS Variant	cDNA.Change	ACMG	ClinVar iD	ParSE-seq P	AC	AF	SpliceAI	PS3	BS3	PM2	PP3	BP4	Result
3-38599058-C-T	c.1891-8G>A	CI	165153	0	18	1.18E-04	0.01	0	1	0	0	1	LB
3-38597840-C-T	c.2151G>A	CI	345125	0	16	1.05E-04	0.00	0	1	0	0	1	LB
3-38597732-G-A	c.2259C>T	CI	345123	0	5	3.28E-05	0.05	0	1	0	0	1	LB
3-38586046-G-T	c.2437-5C>A	CI	139054	0	70	4.60E-04	0.01	0	1	0	0	1	LB
3-38576788-A-G	c.3391-7T>C	CI	345118	0	14	9.20E-05	0.00	0	1	0	0	1	LB
3-38620959-G-A	c.495C>T	CI	378538	0	4	2.63E-05	0.05	0	1	0	0	1	LB
3-38566589-A-T	c.3667-7T>A	CI	139059	0	7	4.60E-05	0.01	0	1	0	0	1	LB
3-38566409-G-A	c.3840C>T	CI	629523	0	4	2.63E-05	0.00	0	1	0	0	1	LB
3-38562505-C-T	c.3873G>A	CI	139061	0	169	1.11E-03	0.00	0	1	0	0	1	LB
3-38560222-G-A	c.4170C>T	CI	518780	0	17	1.12E-04	0.11	0	1	0	0	1	LB
3-38609951-G-A	c.717C>T	CI	48316	0	591	3.88E-03	0.00	0	1	0	0	1	LB
3-38606741-A-G	c.1068T>C	CI	165156	0	485	3.19E-03	0.00	0	1	0	0	1	LB
3-38606137-G-A	c.1152C>T	CI	139047	0	18	1.18E-04	0.02	0	1	0	0	1	LB
3-38604033-A-T	c.1569T>A	CI	165155	0	488	3.21E-03	0.07	0	1	0	0	1	LB
3-38604027-G-A	c.1575C>T	CI	378877	0	5	3.29E-05	0.03	0	1	0	0	1	LB
3-38598928-G-A	c.2013C>T	CI	194288	0	1	6.57E-06	0.04	0	1	1	0	1	LB
3-38597810-G-A	c.2181C>T	CI	345124	0	1	6.57E-06	0.00	0	1	1	0	1	LB
3-38585958-C-A	c.2520G>T	CI	925221	0	2	1.31E-05	0.00	0	1	1	0	1	LB
3-38586048-A-G	c.2437-7T>C	CI	560718	0	0	0.00E+00	0.00	0	1	1	0	1	LB
3-38576784-A-G	c.3391-3T>C	CI	378545	0	2	1.31E-05	0.00	0	1	1	0	1	LB
3-38575454-A-G	c.3512-3T>C	CI	838712	0	1	6.57E-06	0.00	0	1	1	0	1	LB
3-38566451-G-A	c.3798C>T	CI	629343	0	3	1.97E-05	0.00	0	1	1	0	1	LB
3-38566508-T-C	c.3741A>G	CI	962858	0	2	1.31E-05	0.03	0	1	1	0	1	LB
3-38560384-G-A	c.4008C>T	CI	378920	0	2	1.31E-05	0.09	0	1	1	0	1	LB
3-38557288-G-A	c.4246-4C>T	CI	519246	0	1	6.57E-06	0.09	0	1	1	0	1	LB
3-38606774-G-A	c.1035C>T	CI	264022	0	1	6.57E-06	0.15	0	1	1	0	1	LB
3-38604756-A-C	c.1491T>G	CI	345128	0	2	1.31E-05	0.01	0	1	1	0	1	LB
3-38603781-G-A	c.1821C>T	CI	201416	0	3	1.97E-05	0.00	0	1	1	0	1	LB
3-38554373-G-A	c.4719C>T	CI	263423	1	0	0.00E+00	0.90	1	0	1	1	0	LP
3-38566397-G-A	c.3840+12C>T	CI	1327133	0	18	1.18E-04	0.35	0	1	0	0	0	VUS
3-38557234-C-T	c.4296G>A	CI	463336	0	5	3.28E-05	0.43	0	1	0	0	0	VUS
3-38579454-C-G	c.3267G>C	CI	809446	0	0	0.00E+00	0.21	0	1	1	0	0	VUS
3-38560321-C-T	c.4071G>A	CI	406438	0	3	1.97E-05	0.69	0	1	1	1	0	VUS
3-38613816-C-T	c.630G>A	CI	36766	1	92	6.05E-04	0.27	1	0	0	0	0	VUS
3-38575293-G-C	c.3666+4C>G	VUS	926157	0	1	6.57E-06	0.01	0	1	1	0	1	LB
3-38605948-C-T	c.1338+3G>A	VUS	496570	0	0	0.00E+00	0.18	0	1	1	0	1	LB
3-38620838-C-T	c.611+5G>A	VUS	645777	1	0	0.00E+00	0.87	1	0	1	1	0	LP
3-38599055-G-C	c.1891-5C>G	VUS	201463	1	0	0.00E+00	0.98	1	0	1	1	0	LP
3-38560172-G-C	c.4220C>G	VUS	846026	1	0	0.00E+00	0.59	1	0	1	1	0	LP
3-38613744-T-G	c.702A>C	VUS	201442	1	0	0.00E+00	0.69	1	0	1	1	0	LP
3-38557225-A-T	c.4299+6T>A	VUS	229234	1	0	0.00E+00	0.74	1	0	1	1	0	LP
3-38554274-C-T	c.4813+5G>A	VUS	1326912	1	0	0.00E+00	0.94	1	0	1	1	0	LP
3-38608217-G-C	c.935-3C>G	VUS	1326908	1	0	0.00E+00	0.96	1	0	1	1	0	LP
3-38606668-C-T	c.1140+1G>A	VUS	180520	1	0	0.00E+00	0.99	1	0	1	1	0	LP
3-38605951-C-T	c.1338G>A	VUS	451631	1	0	0.00E+00	0.95	1	0	1	1	0	LP
3-38603713-G-A	c.1889C>T	VUS	201462	0	11	7.23E-05	0.11	0	0	0	0	1	VUS
3-38604025-C-T	c.1577G>A	VUS	67668	0	8	5.26E-05	0.23	0	0	0	0	0	VUS
3-38604907-G-C	c.1340C>G	VUS	67657	0	32	2.10E-04	0.01	0	0	0	0	1	VUS
3-38604064-C-G	c.1538G>C	VUS	532073	0	0	0.00E+00	0.21	0	0	1	0	0	VUS
3-38604019-C-A	c.1583G>T	VUS	406425	0	0	0.00E+00	0.25	0	0	1	0	0	VUS
3-38597740-C-T	c.2251G>A	VUS	923998	0	1	6.57E-06	0.20	0	0	1	0	0	VUS
3-38597730-A-T	c.2261T>A	VUS	406449	0	0	0.00E+00	0.20	0	0	1	0	1	VUS
3-38575451-C-T	c.3512G>A	VUS	242195	0	0	0.00E+00	0.01	0	0	1	0	1	VUS
3-38575299-G-A	c.3664C>T	VUS	919970	0	0	0.00E+00	0.35	0	1	1	0	0	VUS
3-38566432-A-C	c.3817T>G	VUS	651986	0	0	0.00E+00	0.20	0	0	1	0	1	VUS
3-38613791-G-A	c.655C>T	VUS	432157	0	0	0.00E+00	0.34	0	0	1	0	0	VUS
3-38560388-A-C	c.4004T>G	VUS	923272	0	0	0.00E+00	0.39	0	0	1	0	0	VUS
3-38560200-C-T	c.4192G>A	VUS	1482306	0	0	0.00E+00	0.28	0	0	1	0	0	VUS
3-38557248-C-A	c.4282G>T	VUS	179030	0	1	6.57E-06	0.27	0	0	1	0	0	VUS
3-38557250-G-T	c.4280C>A	VUS	519279	0	0	0.00E+00	0.23	0	0	1	0	0	VUS
3-38557234-C-A	c.4296G>T	VUS	659965	0	0	0.00E+00	0.41	0	0	1	0	0	VUS
3-38554380-A-C	c.4712T>G	VUS	67917	0	0	0.00E+00	0.21	0	0	1	0	0	VUS
3-38554377-G-C	c.4715C>G	VUS	1055232	0	0	0.00E+00	0.30	0	0	1	0	0	VUS
3-38554368-C-T	c.4724G>A	VUS	532081	0	0	0.00E+00	0.30	0	0	1	0	0	VUS

3-38554318-T-A	c.4774A>T	VUS	583356	0	0	0.00E+00	0.41	0	0	1	0	0	VUS
3-38609836-G-A	c.832C>T	VUS	1171664	0	0	0.00E+00	0.32	0	0	1	0	0	VUS
3-38620843-G-A	c.611C>T	VUS	68028	0	2	1.31E-05	0.07	0	0	1	0	1	VUS
3-38606151-GG-TA	c.1141-4_1141-3delinsTA	VUS	569946	0	0	0.00E+00	0.00	0	1	1	0	0	VUS
3-38620844-C-T	c.610G>A	VUS	633409	0	0	0.00E+00	0.02	0	0	1	0	1	VUS
3-38604730-A-T	c.1517T>A	VUS	809450	0	1	6.57E-06	0.19	0	0	1	0	1	VUS
3-38604848-C-A	c.1399G>T	VUS	201454	0	0	0.00E+00	0.31	0	0	1	0	0	VUS
3-38604790-G-C	c.1457C>G	VUS	853715	0	0	0.00E+00	0.20	0	0	1	0	1	VUS
3-38575399-C-A	c.3564G>T	VUS	1430298	0	2	1.31E-05	0.62	0	1	1	1	0	VUS
3-38560345-GCTGAAGATGAGC-G	c.4032_4043del	VUS	1377833	0	0	0.00E+00	0.53	0	0	1	1	0	VUS
3-38609832-T-C	c.836A>G	VUS	1406965	0	0	0.00E+00	0.66	0	0	1	1	0	VUS
3-38576780-G-A	c.3392C>T	VUS	67795	1	14	9.19E-05	0.00	1	0	0	0	1	VUS
3-38599058-C-T	c.1891-8G>A	CI	165153	0	18	1.18E-04	0.01	0	1	0	0	1	LB

Supplementary Table 6. Normalized electrophysiologic Data for two $Na_V1.5$ variants. Standard error of the mean is shown in parentheses for raw values.

Variant	Normalized Peak Density	Cells	
A1407G	121.9 (9.1)	46	
T1131I	94 (7.3)	67	
	Mean V_act	**Cells**	**Normalized Mean**
A1407G	-64 (3.7)	5	-20
T1131I	-58 (2.3)	16	-14
	Mean Tau_inactivation	**Cells**	**Normalized Mean**
A1407G	1.431 (0.069)	45	-0.343
T1131I	1.069 (0.033)	50	-0.705
	Mean V_inact	**Cells**	**Normalized Mean**
A1407G	-107.1 (2.4)	5	-8.7
T1131I	-110.2 (2.0)	20	-11.8
	Recovery from Inact 50	**Cells**	**Normalized Mean**
A1407G	20.4 (1.0)	5	9
T1131I	22.3 (2.6)	18	10.9
	Late Current Ratio (50 ms)	**Cells**	
A1407G	0.0038 (0.00009)	15	
T1131I	0.0017 (0.00009)	21	

Supplementary Table 7. Passive parameters of iPSC-CM manual patch-clamp experiments. Recorded parameters are presented for each cell. Cell capacitance and membrane resistance are provided for all single cells used in this study. Since the current study focused on I_{Na} measurements under modified experimental conditions (see Methods), current-clamp mode was not able to accurately monitor membrane potentials. †Membrane potential from previously published data by our laboratory[4]. † indicates $p > 0.05$, no statistically significant difference among groups from an unpaired two-sided t-test without adjustment for multiple testing.

Membrane potential (mV) †														
Cell#	**1**	**2**	**3**	**4**	**5**	**6**	**7**	**8**	**9**	**10**	**11**	**12**	**13**	**Summary (mV)**
WT	-75	-77.6	-81.3	-81.4	-84.5	-80.4	-82.8	-90	-87.3	-78.6	-86.3	-84.6	-78.6	-82.2±1.2
Capacitance (pF)														
Cell#	**1**	**2**	**3**	**4**	**5**	**6**	**7**	**8**	**9**	**10**	**11**	**12**	**13**	**Summary (pF) †**
WT	46.3	42.6	38.9	72.3	41.5	56.2	50.6	70.5	67.8	82.5				56.9±4.8
c.4220c>G	47.2	48.3	45.6	46.8	43.8	44.5	47.3	48.9	46.2	40.2				45.9±0.8
c.1891-5C>G	47.3	50.3	51.3	46.8	41.6	44.5	67.4	68.2	46.5	43.7	46.2	53.6		50.6±2.5
Membrane resistance (GΩ)														
Cell#	**1**	**2**	**3**	**4**	**5**	**6**	**7**	**8**	**9**	**10**	**11**	**12**	**13**	**Summary (GΩ) †**
WT	1	1.2	1.8	1.4	1.6	1.5	2	1.6	1.7	1.6				1.54±0.09
c.4220c>G	1.6	1	1.4	1.8	1.9	2	1.7	1.6	1.3	1.2				1.55±0.1
c.1891-5C>G	1.1	1	1.4	1.5	1.8	2	1.6	1.4	1.9	1.4	1.8	1.5		1.53±0.08

Supplementary References.

1 O'Neill, M. J. *et al.* Functional Assays Reclassify Suspected Splice-Altering Variants of Uncertain Significance in Mendelian Channelopathies. *Circ Genom Precis Med*, 101161circgen122003782 (2022). https://doi.org/10.1161/circgen.122.003782

2 Battle, A., Brown, C. D., Engelhardt, B. E. & Montgomery, S. B. Genetic effects on gene expression across human tissues. *Nature* **550**, 204-213 (2017). https://doi.org/10.1038/nature24277

3 Brnich, S. E. *et al.* Recommendations for application of the functional evidence PS3/BS3 criterion using the ACMG/AMP sequence variant interpretation framework. *Genome Med* **12**, 3 (2019). https://doi.org/10.1186/s13073-019-0690-2

4 Bersell, K. R. *et al.* Transcriptional Dysregulation Underlies Both Monogenic Arrhythmia Syndrome and Common Modifiers of Cardiac Repolarization. *Circulation* (2022). https://doi.org/10.1161/circulationaha.122.062193